Radiation Stability of Cations in Ionic Liquids. 4. Task-Specific Antioxidant Cations for Nuclear Separations and Photolithography

ARTICLE *in* THE JOURNAL OF PHYSICAL CHEMISTRY B · NOVEMBER 2013

Impact Factor: 3.3 · DOI: 10.1021/jp408252n · Source: PubMed

2 AUTHORS:

Ilya Shkrob
Argonne National Laboratory
143 PUBLICATIONS **2,164** CITATIONS

SEE PROFILE

Timothy W Marin
Benedictine University
54 PUBLICATIONS **810** CITATIONS

SEE PROFILE

THE JOURNAL OF PHYSICAL CHEMISTRY B

Article

pubs.acs.org/JPCB

Radiation Stability of Cations in Ionic Liquids. 4. Task-Specific Antioxidant Cations for Nuclear Separations and Photolithography

Ilya A. Shkrob*[,†] and Timothy W. Marin[†,‡]

[†]Chemical Sciences and Engineering Division, Argonne National Laboratory, 9700 South Cass Avenue, Argonne, Illinois 60439, United States

[‡]Chemistry Department, Benedictine University, 5700 College Road, Lisle, Illinois 60532, United States

Supporting Information

ABSTRACT: Three families of "task-specific" antioxidant organic cations that include designated sites to facilitate deprotonation following electronic excitation and ionization have been introduced. The deprotonation from the excited state is reversible, leading to minimal damage of the cation, whereas the deprotonation from the oxidized cation yields persistent aroxyl and trityl radicals. This protection improves radiation stability of ionic compounds in 2.5 MeV electron beam radiolysis. Apart from the use of such cations as structural components of room temperature ionic liquid (IL) diluents for nuclear separations, their ionic compounds involving bases of superacids are well suited for use as chemically amplified acid generator resists in electron beam lithography and extreme ultraviolet photolithography.

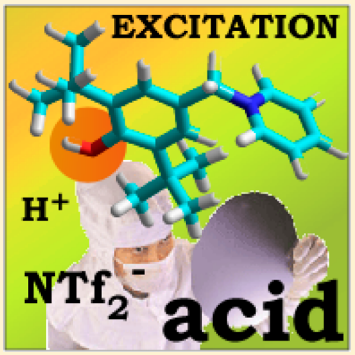

1. INTRODUCTION

In parts 1,[1] 2,[2] and 3[3] of this series, the radiation stability of commonly used organic cations in ionic liquid (IL) diluents[4−6] was examined. Such diluents are being considered for advanced nuclear separations.[7−14] This application requires the use of radiation-hard ions, as gradual decomposition of IL solvent by decaying radionuclides in spent fuel interferes with radionuclide separations.[15−17] However, what makes a material unsuitable for one application sometimes makes it suitable for another application, and vice versa. In part 4, we explore this connection.

Since the pioneering studies of Crivello and co-workers,[18−22] ionic compounds ($\mathbf{C^+A^-}$) involving conjugate bases of superacids ($H^{\delta+}\mathbf{A}^{\delta-}$) found wide use as chemically amplified acid generator resists. The typical anions used in such photoresists are triflate (TfO^-, where Tf = CF_3SO_2), SbF_6^-, AsF_6^-, BF_4^-, and PF_6^-.[18,23,24] Photo- and radiation-induced generation of strong acids in a polymeric matrix (that undergoes acid catalyzed decomposition) serves as the chemical basis for high resolution lithography in microchip manufacturing.[24−27] A chemical world apart, hydrophobic ILs composed of similar compounds are being considered as replacements for molecular diluents in nuclear separations.[13] Since at some point in the extraction cycle the IL diluents are placed in contact with strong acids in the aqueous raffinate, the constituent hydrophobic anions are conjugate bases of superacids, such as hexafluorophosphate (PF_6^-) and bistriflimide (NTf_2^-), which are used in order to avoid protonation of these constituent anions and reconstitution of the IL.[28] In one application (resists) photo/radiolytic damage is desired and in another (nuclear separations) it needs to be avoided, yet the underlying chemistry is the same. Can lessons learned in one field be used to address outstanding challenges in the other field?

A common property of organic cations is that their excitation frequently results in the elimination of side arms through dissociation of carbon−heteroatom bonds.[1−3,29,30] Considering a typical photoresist cation, such as arylsulfonium (R_2S^+Ar, Scheme 1), ultraviolet (UV) excitation causes the release of carbocations and/or radical cations[31,32]

Scheme 1. Photoacid Generation from Arylsulfonium Resists

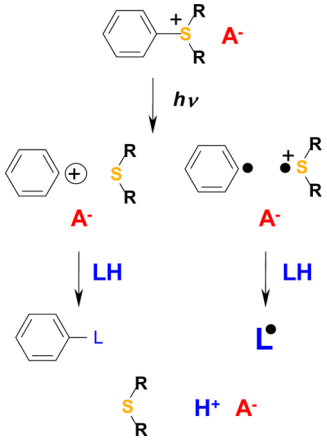

Received: August 18, 2013
Revised: November 7, 2013
Published: November 8, 2013

$$R_2S^+Ar + h\nu \rightarrow R_2S + Ar^+ \quad (1a)$$

$$R_2S^+Ar + h\nu \rightarrow R_2S^{+\bullet} + Ar^\bullet \quad (1b)$$

The resulting carbocation (Ar^+) and radical cation ($R_2S^{+\bullet}$) react with the parent cation by attaching to an aromatic ring of the parent cation or the substrate (reaction 2a) or abstract H from a polymer substrate (**LH**, reaction 2b)

$$Ar^+\mathbf{A}^- + \mathbf{LH} \rightarrow Ar\mathbf{L} + H^{\delta+}\mathbf{A}^{\delta-} \quad (2a)$$

$$R_2S^{+\bullet}\mathbf{A}^- + \mathbf{LH} \rightarrow R_2S + H^{\delta+}\mathbf{A}^{\delta-} + \mathbf{L}^\bullet \quad (2b)$$

yielding superacids (Scheme 1). These ionic compounds are *crystalline solids* that can be purified by repeated recrystallization (as high purity is desired). In contrast, IL based diluents are *hydrophobic fluids*.[4,5] The fragmentation reactions responsible for photoacid generation via reactions 2a and 2b also cause irreversible decay of IL cations during radiolysis. Although sulfonium salts are not used as IL diluents, the same problem occurs for cyclic and acyclic onium,[33,34] imidazolium,[1,29,35,36] pyridinium,[2] guanidinium[3] and other organic cations.[30] While the dissociative states of such cations cannot be accessed with low-energy ultraviolet light, these states are generated by ionizing radiation, including focused electron beams and EUV (extreme ultraviolet) light which are used for nanometer resolution lithography in the electronics industry.[27]

Originally,[18] another strategy for photoacid generation had been considered, namely, the use of strategically placed deprotonation sites. For instance, UV photolysis of hydroxylated arylsulfonium cations (Scheme 2) causes their deprotonation from the hydroxyl group with the formation of a zwitterion:[18−20,22,37]

Scheme 2. Deprotonation in Excited Hydroxylated Arylsulfonium

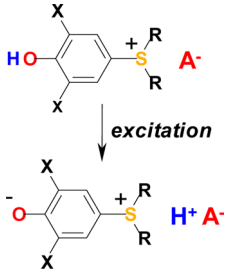

$$HOArS^+R_2\mathbf{A}^- + h\nu \rightarrow H^{\delta+}\mathbf{A}^{\delta-} + O^-ArS^+R_2 \quad (3)$$

In this manner, weak $S-C_1$ bonds in an arysulfonium cation (structure **1a** in Scheme 3) can be protected by channeling of the excitation energy to a still weaker O−H bond in the aroxyl unit. In the absence of polymeric substrate to protonate, this photoreaction is reversible, which makes it interesting from the standpoint of radiation protection of IL solvents used for nuclear separations.

The usefulness of such deprotonation sites is not limited to the suppression of reactions 1a and 1b. Energetic excitation of cations ($\mathbf{C}^+$) also causes electron detachment from these cations, generating unstable radical dications, $\mathbf{C}^{2+\bullet}$.[29,30,33] These species promptly deprotonate, typically from their aliphatic arms, generating acids;[38,39] the gross reaction can be written as

$$\mathbf{C}^+\mathbf{A}^+ \rightarrow\rightarrow e^{-\bullet} + \mathbf{C}(-H)^{+\bullet} + H^{\delta+}\mathbf{A}^{\delta-}$$

Scheme 3. Structural Formulas for Organic Cations with Dedicated Deprotonation Sites

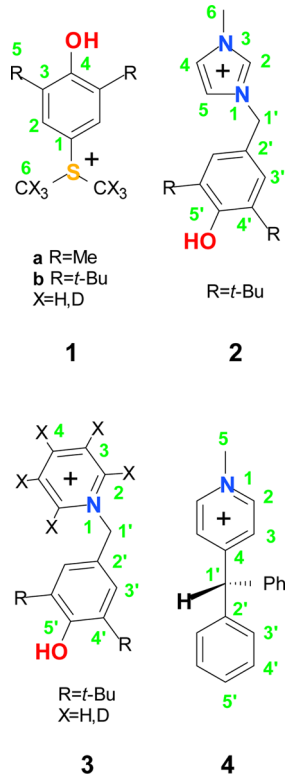

The resulting $\mathbf{C}(-H)^{+\bullet}$ radicals recombine with other radiolytically generated radicals, leading to oligomerization and chemical modification of the parent cations.[29,40] If this deprotonation is channeled to a particular site in the cation, this secondary chemistry can be suppressed provided that the $\mathbf{C}(-H)^{+\bullet}$ radicals are unreactive. For example, crowded aryloxy ($-ArO^\bullet$) radicals can be very stable,[41] and many antioxidants and "antirads" (sacrificial agents that are used to reduce radiolytic or oxidative damage) involve −ArOH groups.[42] Conversely, when a substituted Ar_2CH- group (as in structure **4** in Scheme 3) is used as the deprotonation site, the resulting trityl radical is generated as another sterically hindered, persistent radical.[43]

In this study, we examine the radiation stability of three classes of cations that include such deprotonation sites (Scheme 3). Structures **1a** and **1b** are inspired by Crivello's photoresists (reaction 3).[22] Structures **2** and **3** are 5′-hydroxy modifications of the 1-benzyl-3-methylimidazolium ($BzMeIm^+$) and 1-benzylpyridinium ($BzPy^+$) compounds we studied in parts 1 and 2 of this series, respectively.[1,2] For these cations, electronic excitation caused elimination of Bz^+ carbocation. While the latter reaction (analogous to reaction 1a) is reversible, there was significant loss of Bz^+ carbocations through the addition of the latter to the benzyl group of parent cations.[2] We reasoned that, in cations **2** and **3**, O−H bond dissociation may be more facile than this $N_1-C_{1'}$ bond dissociation, preventing the occurrence of the latter. In structure **4**, the N−Me bond was expected to avoid dissociation that is typical of the N-alkyl groups involving longer aliphatic arms[30] that decompose to $>NH^+$ cation and 1-olefin. Since cation **4** can readily deprotonate at carbon-1′ in the excited and oxidized states, we speculated that this cation would exhibit greater resilience to radiation.

dx.doi.org/10.1021/jp408252n | J. Phys. Chem. B 2013, 117, 14797−14807

Our approach exemplifies the use of "task-specific" ionic compounds,[44,45] in which organic ions are chemically tailored to accomplish specific tasks, such as metal ion extraction,[7,46,47] biopolymer and oxide[48,49] dissolution, nanoparticle stabilization,[46,50] CO_2 capture,[46] chemical catalysis,[45,46,50] etc. In our case, the related "tasks" are (i) improving radiation/oxidation stability of IL diluents and (ii) increasing the efficiency of deprotonation in ionic compounds exposed to energetic radiation for lithography. To save space, many of the supporting tables, figures, details of synthetic and analytical protocols, and a list of abbreviations have been placed in the Supporting Information. When referenced in the text, these materials have the designator "S", as in Figure 1S. The atom numbering used in Scheme 3 is followed throughout the text.

2. EXPERIMENTAL AND COMPUTATIONAL METHODS

Synthetic procedures are given in section 1S in the Supporting Information. All starting materials were obtained from Aldrich. Hexafluorophosphate (PF_6^-), tetrafluoroborate (BF_4^-), triflate (TfO^-), bistriflimide (NTf_2), and saccharinate (Sac^-) compounds were synthesized. Chlorides of **1a** and **1b** ($HOArS^+(CX_3)_2$, where X = H, D) were synthesized following the method of Crivello and Lam[18] from the corresponding phenols and $OS(CX_3)_2$ in HCl/1,4-dioxane. The chloride salt was multiply recrystallized from acetonitrile and then metathesized in aqueous solutions containing alkali salts of the desired anions. Tetrafluoroborates of **2** and **3** ($MeIm\text{-}CH_2ArOH^+$ and $PyCH_2ArOH^+$, respectively) were synthesized from pyridinium (-h_5 or -d_5) and 1-methylimidazolium tetrafluoroborates and 3,5-di-*tert*-butyl-4-hydroxybenzyl alcohol in the Mitsunobu reaction.[51,52] Cation **4** was obtained by quaternization of diphenyl-4-pyridylmethane.[53,54] All of the ionic compounds were crystalline, including the bistriflimides (e.g., see the crystal structure for **1b** NTf_2 in section 2S and Figure 1S, Supporting Information). This allowed us to achieve high purity through the use of multiple recrystallization. The melting/decomposition points are given in Table 1S (Supporting Information); Table 2S (Supporting Information) lists the mass peaks, and Figures 2S−6S (Supporting Information) summarize ^1H and ^{13}C NMR spectra.

The experimental and computational approaches were similar to these used in parts 1 and 2 of this study.[1,2] For product analysis, the samples were evacuated and sealed in water-cooled borosilicate NMR tubes (O.D. 5 mm) and irradiated by 2.5 MeV electrons to a total dose of ∼3.2 MGy using a dose rate of 6.8 kGy/s (1 Gy = 1 J/kg of the absorbed energy). ^1H and ^{13}C NMR spectra were obtained in dimethylsulfoxide-d_6 (DMSO-d_6), using an Avance DMX 500 MHz spectrometer (Bruker). $^1H-^1H$ COSY spectroscopy was used to establish proton connectivity. For ^{19}F and ^{31}P NMR, the chemical shifts are given relative to $CFCl_3$ and H_3PO_3 standards, respectively.

Tandem electrospray ionization mass spectra (ESI MS_n) were obtained using a Thermo Scientific LCQ Fleet ion trap mass spectrometer operating either in positive or negative modes ($MS_n^{\pm}$). MS_1 corresponds to the first quadrupole, and MS_2 corresponds to collision induced dissociation (of mass selected ions) modes of operation. Liquid samples were injected directly into dilute acetonitrile solutions. $(\mathbf{CA})_n\mathbf{C}^+$ and $(\mathbf{CA})_n\mathbf{A}^-$ cluster ion series were detected (hereafter, $\mathbf{C}^+$ and $\mathbf{A}^-$ are the constituent ions). In section 3.2, only $n = 0$ ions of each series are reported. For analysis, radiolyzed samples were dissolved in acetonitrile to obtain 1−2 wt % solutions. High performance liquid chromatography-mass spectrometry (LCMS) was used to separate and identify isobaric products. To this end, a 2 μL aliquot was analyzed using reverse phase chromatography (ThermoScientific Accela suit) with ESI MS_1^+ detection (the same MS instrument). A weak cation exchange phase with carboxylate surface groups was used (Thermo Scientific WCX-1 phase; 120 Å pore, size 3 μm; 3 mm bore, 15 cm length) for isothermal elution at 0.2 mL/min; acetonitrile containing 0.1 wt % formic acid was used as an eluent.

For EPR spectroscopy, the samples were frozen by rapid immersion in liquid nitrogen and irradiated to 3 kGy at 77 K. The radicals were observed using a 9.44 GHz Bruker ESP300E spectrometer, with the sample placed in a flow helium cryostat (Oxford Instruments CF935). The magnetic field and the hyperfine coupling constants (hfcc's) are given in the units of Gauss (1 G = 10^{-4} T). If not stated otherwise, the first-derivative EPR spectra were obtained at 50 K using 2 G modulation at 100 kHz. The microwave power is indicated in the figures. The radiation-induced EPR signal from the E_γ' center in the Suprasil sample tubes (that frequently overlapped with the resonance lines of organic radicals) is shadowed white in some of the EPR spectra. The calculations of hyperfine coupling (hfcc) tensors **A** and radical structures were carried out using a density functional theory (DFT) method with the B3LYP functional[55,56] and 6-31+G(d,p) basis set from Gaussian 03.[57] In the following, a_{iso} denotes the isotropic hfc constant (hfcc) corresponding to the hfc tensor and **B** denotes the anisotropic part of this tensor. Powder EPR spectra were simulated using first-order perturbation theory assuming isotropic **g**-tensors.

3. RESULTS AND DISCUSSION

3.1. EPR Studies of Radiation Induced Redox Reactions.

3.1.1. 1-(3,5-Ditert-butyl-4-hydroxybenzyl)-3-methylimidazolium and 1-(3,5-Ditert-butyl-4-hydroxybenzyl)pyridinium. In parts 1 and 2,[1,2] radiolysis of 1-benzyl-3-methylimidazolium ($BzMeIm^+$) and 1-benzylpyridinium ($BzPy^+$) cations was studied. One-electron reduction of the $BzMeIm^+$ cation caused the elimination of benzyl radical ($Bz^\bullet$)[1]

$$BzMeIm^+ + e^{-\bullet} \rightarrow MeIm + Bz^\bullet \quad (4a)$$

while the reduction of $BzPy^+$ yielded the $(BzPy)_2^{+\bullet}$ dimer radical cation in which the excess electron is shared by π-stacked pyridinium moieties in a sandwich configuration.[2] Radiolytic oxidation of $MeImBz^+$ results in the formation of H loss radical at carbon-1′,[1] whereas the oxidation of $BzPy^+$ yielded stable $(BzPy)_2^{3+\bullet}$ radical trications.[2] For the $\mathbf{B}^+CH_2ArOH$ cations (where **B** is the aromatic base), one can expect similar chemistry, including a reaction analogous to reaction 4a

$$\mathbf{B}^+CH_2ArOH + e^{-\bullet} \rightarrow \mathbf{B} + {}^\bullet CH_2ArOH \quad (4b)$$

and we used DFT to calculate several conformers of the corresponding gas-phase radicals (**B** = Py, Figure 7S, Supporting Information) and simulate their EPR spectra (Figures 8S and 9S, Supporting Information). See Table 3S (Supporting Information) for energetics and Table 4S (Supporting Information) for the summary of hfcc's. In addition to the electron adducts and $H_{1'}$ loss (reaction 5a below), one can expect deprotonation of the oxidized cations from the hydroxyl group (reaction 5b), as the estimated

dx.doi.org/10.1021/jp408252n | J. Phys. Chem. B 2013, 117, 14797−14807

energies of the $C_{1'}$–H and O–H bonds in the cation are 3.86 and 3.94 eV, respectively (Scheme 4):

$$\mathbf{B}^{+}CH_2ArOH\ \mathbf{A}^{-} \rightarrow\rightarrow e^{-\bullet} + \mathbf{B}^{+}C^{\bullet}HArOH + H^{\delta+}\mathbf{A}^{\delta-} \quad (5a)$$

$$\mathbf{B}^{+}CH_2ArOH\ \mathbf{A}^{-} \rightarrow\rightarrow e^{-\bullet} + \mathbf{B}^{+}CH_2ArO^{\bullet} + H^{\delta+}\mathbf{A}^{\delta-} \quad (5b)$$

Scheme 4. Possible Oxidation and Reduction Pathways for Cations 2 and 3[a]

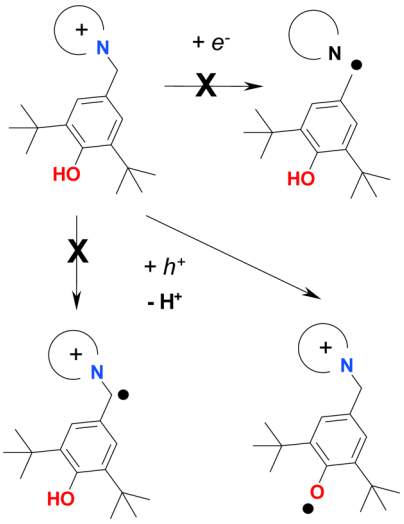

[a]Crossed pathways are excluded by EPR spectroscopy.

As seen from Figure 9S (Supporting Information), these H loss radicals and $^{\bullet}CH_2ArOH$ radicals have easily distinguishable EPR spectra. As the electron adducts have unpaired electron density mainly on their heterocycle rings, these species (2-imidazolyl and pyridinyl radicals) can be distinguished through a characteristic narrowing of their EPR spectrum upon perdeutero substitution in these heterocycle bases (Figure 8S and Table 4S, Supporting Information). Our DFT calculations suggest that such radicals are even more unstable with regard to $C_{1'}$–N_1 bond dissociation reaction 4b than the corresponding benzyl derivatives (Table 3S, Supporting Information) due to increased stability of the outgoing $^{\bullet}CH_2ArOH$ radical. For the same reason, the elimination of the $^{+}CH_2ArOH$ carbocation is ~1 eV less endergonic than the elimination of Bz^{+} from $BzPy^{+}$ (Table 3S, Supporting Information).

Figure 1a shows EPR spectra obtained for irradiated frozen MeImCH$_2$ArOH BF_4. Qualitatively, this EPR spectrum consists of two contributions: (i) a doublet of closely spaced lines (that exhibit ~8.6 G spacing) indicated by the arrows in the plot and (ii) an unresolved singlet at the center of the spectrum (with peak-to-peak spacing ΔB_{pp} of 15.2 G). This doublet corresponds to $M(2^1H) = \pm 1$ lines (a_{iso} ~ 55 G) in an H atom adduct at carbon-2 of the imidazolium ring, and the additional structure observed in these lines is also consistent with this attribution[1,29,58,59] Such radical cations have been observed in other tetrafluoroborate compounds,[1,59] which have significant protic impurity (as these compounds are synthesized from HBF_4). Importantly, the –ArOH group itself is a weak acid, and the phenols are known to react with solvated electrons in saturated hydrocarbons, subsequently releasing $H^{\bullet}$ atoms (and yielding H atom adducts).[60] It appears that either

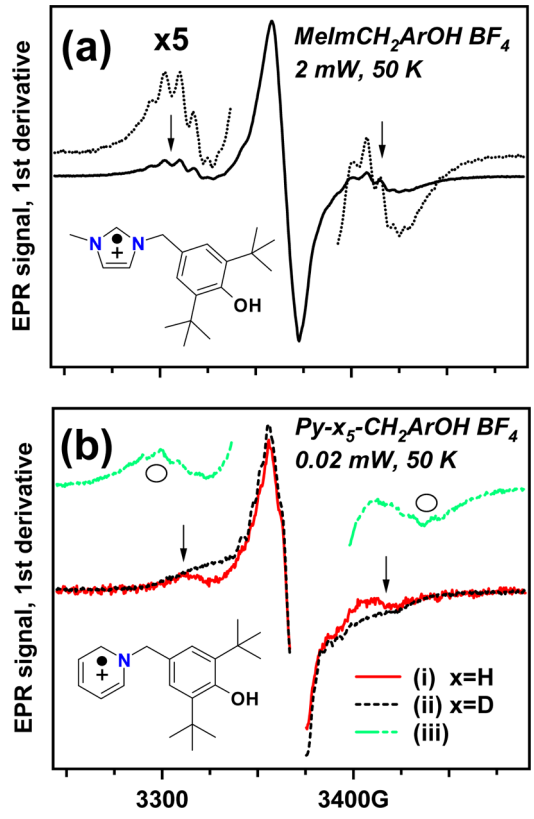

Figure 1. First-derivative EPR spectra of irradiated frozen (a) MeImCH$_2$ArOH BF_4 and (b) Py-x_5-CH$_2$ArOH BF_4 (x = (i) H (solid line) or (ii) D (dashed line)) observed at 50 K. The $M(2^1H) = \pm 1$ lines from 2,2′ hydrogen atom adducts shown in the insets are indicated by the arrows. In trace iii (panel b), the analogous resonances for pyridinium are indicated by the open circles.

(i) the electrons are trapped by protic impurity, yielding the $H^{\bullet}$ atoms that add to the imidazolium ring (or abstract H from the hydroxyl groups of the parent cation), or (ii) the electron adduct is protonated

$$\mathbf{C} + e^{-\bullet} \rightarrow \mathbf{C}^{\bullet}$$

$$\mathbf{C}^{\bullet} + H^{\delta+}\mathbf{A}^{\delta-} \rightarrow \mathbf{C}H^{+\bullet}\mathbf{A}^{-}$$

before it dissociates via reaction 4b.[29] The H loss radical (Scheme 4) from the carbon-1′ site is not observed; also, there is no indication for C–N bond dissociation that yields the $^{\bullet}CH_2ArOH$ radical (Figures 9S and 10S, Supporting Information). The radicals shown in Figure 1a are stable even at 300 K, which excludes the electron adducts as progenitors of the singlet. The latter is from the aroxyl radical MeIm-$CH_2ArO^{\bullet}$, which is also suggested by intense blue coloration of irradiated material.

Figures 1b and 11S (Supporting Information) exhibit the EPR spectra for irradiated Py-x_5-CH$_2$ArOH BF_4 compounds (x = H, D). This EPR spectrum also exhibits a 110 G doublet (indicated by the arrows in the plot) and the singlet resonance line at the center (with ΔB_{pp} ~ 18 G). This doublet is not observed after d_5-substitution in the pyridinium group, which is consistent with the formation of the 2,2′-(H,D) adduct (the carbon-2 site is suggested in analogy to $BzPy^{+}$).[2] Such H atom adducts, albeit with a larger $a_{iso}(^1H)$, have been observed in radiolysis of PyH BF_4 (the upper trace in Figure 1b). The singlet line does not change upon this d_5-substitution, so it

dx.doi.org/10.1021/jp408252n | J. Phys. Chem. B 2013, 117, 14797–14807

cannot originate from the electron adducts (Figure 8S, Supporting Information). Warming of the sample to 300 K causes gradual decay of these radicals. The H atom adduct fully decays at 300 K, whereas the other radical persists. We identify this persistent species as the aroxy radical, judging both from its color and the observed EPR pattern. We conclude that in cations **2** and **3** the deprotonation proceeded mainly from the hydroxyl group. There is no evidence for homolytic $C_{1'}$–N_1 bond dissociation.

3.1.2. 1-Methyl-4-diphenylmethylpyridinium. Figure 2a exhibits EPR spectra obtained for irradiated ionic compounds

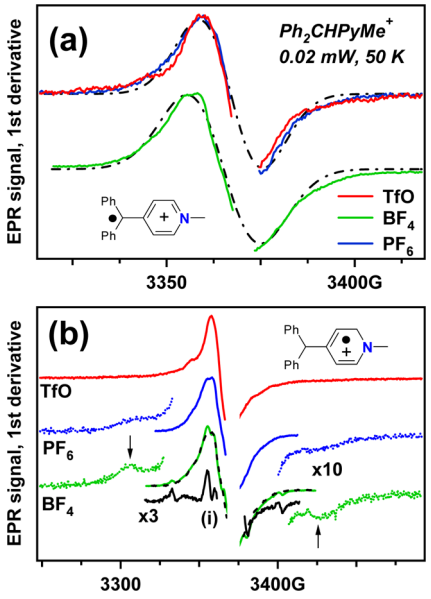

Figure 2. (a) Comparison of normalized EPR spectra from irradiated $Ph_2CHPyMe^+$ compounds (triflate, tetrafluoroborate, and hexafluorophosphate; see the legend). Dashed lines are Gaussian fits to these EPR spectra. The inset shows the progenitor radical. (b) A wider field scan indicating the lines of the corresponding H atom adducts (indicated by the arrows and shown in the inset). For the tetrafluoroborate, subtraction of the Gaussian line indicates the presence of the methyl radical, trace i.

of $Ph_2CHPyMe^+$, cation **4** in Scheme 3. The deprotonation of oxidized cation is expected to yield a stable $Ph_2C^{\bullet}PyMe^+$ radical that is analogous to the well-known trityl radicals.[43] Indeed, in all of these systems, a singlet Gaussian line with $\Delta B_{pp} \sim 18$ G was observed that persisted to 300 K (Figure 12S, Supporting Information). In addition to this feature, there is a doublet of lines indicated by the arrows in Figure 2b that are attributed to the outer lines of an H atom adduct with $a_{iso}(^1H) \sim 60$ G. For the tetrafluoroborate compound, a quartet of narrow lines is discernible (trace i in Figure 2b). This contribution is from the methyl radical, suggesting the occurrence of C_5–N_1 bond dissociation. This methyl radical was not observed in other compounds of **4**. For bistriflimide (Figure 13S, Supporting Information), there was an additional EPR signal overlapping with the Gaussian line that disappeared above 160 K. We observed this feature in some other bistriflimide compounds and attributed it to the $^{\bullet}SO_2NTf^-$ radical anion.[40] The complementary $^{\bullet}CF_3$ radical can be observed in the wings,[33,39] and one of the resonance lines of the $^{\bullet}CF_2SO_3^-$ radical[39] can be observed in the irradiated triflate compound (Figure 13S(a), Supporting Information). These EPR observations suggest that cation **4** is resilient to radiolytic oxidation and reduction, yielding stable radicals.

3.1.3. 3,5-Dialkyl-4-hydroxyphenyldimethylsulfonium. In addition to reactions 1b and 2b, there are several other reactions of cations **1a,b** (Scheme 3) that can yield radicals in radiolysis of the $HOArS^+Me_2$ cations (Figures 14S and 15S, Supporting Information). In addition to the deprotonation from their hydroxyl and alkyl groups, one can expect dissociative electron attachment reactions 6a and 6b (Scheme 5)

$$HOArS^+Me + e^{-\bullet} \rightarrow HOAr^{\bullet} + SMe_2 \quad (6a)$$

$$\rightarrow H^{\bullet} + O^-ArS^+Me_2 \quad (6b)$$

Scheme 5. Chemical Pathways Leading to Radicals Observed in Radiolysis of Cation 1b

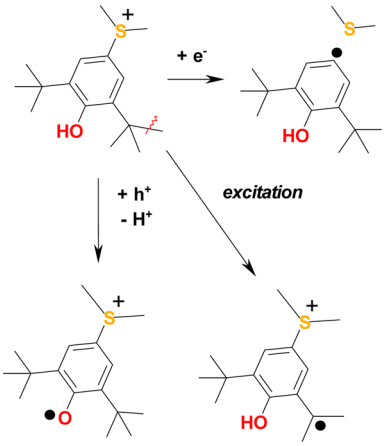

Our DFT calculations summarized in Table 5S and Figure 15S (Supporting Information) indicate that in the gas phase S–C_1 dissociation in the electron adduct of **1a** is exergonic by 0.47 eV (vs 0.39 eV for PhS^+Me_2, see Table 6S, Supporting Information), whereas H atom elimination from the S–Me group is endergonic by 1.69 eV. Reactions analogous to reactions 1a and 1b require excitation to at least 3.78 and 4.31 eV (vs 3.81 and 4.04 eV for PhS^+Me_2), respectively, while the homolytic dissociation of the O–H bond requires ~4.23 eV. Deprotonation from the C_3–Me group is predicted to be slightly more exergonic than deprotonation from the O–H group (bond energy of 4.20 vs 4.23 eV, respectively), while deprotonation from the S–Me group is least favorable (4.79 eV).

In contrast, the loss of the methyl arm via homolytic cleavage is more facile at the sulfur than at carbon-3 (2.23 vs 4.58 eV, respectively). These DFT calculations also suggest that H atom addition to cation **1a** (that can also be regarded as protonation of the corresponding electron adduct) is exergonic by 1.11 eV at carbon-4 and 1.31 eV at carbon-2. In the gas phase, the radical dication is close in energy (Figure 15S, Supporting Information) to $Me_2S^{+\bullet}$ + $^+$ArOH, so S–C_1 bond dissociation can take place *before* the deprotonation. In Figures 16S and 17S (Supporting Information), we simulated EPR spectra of radicals derived from cations **1a** and **1b** using the hfcc parameters given in Tables 7S and 8S (Supporting Information).

Figure 3a shows the EPR spectra of irradiated hexafluorophosphates of cation **1b**-h_6 and **1b**-d_6. As the corresponding EPR spectra are virtually identical, it follows that H atom loss

dx.doi.org/10.1021/jp408252n | J. Phys. Chem. B 2013, 117, 14797–14807

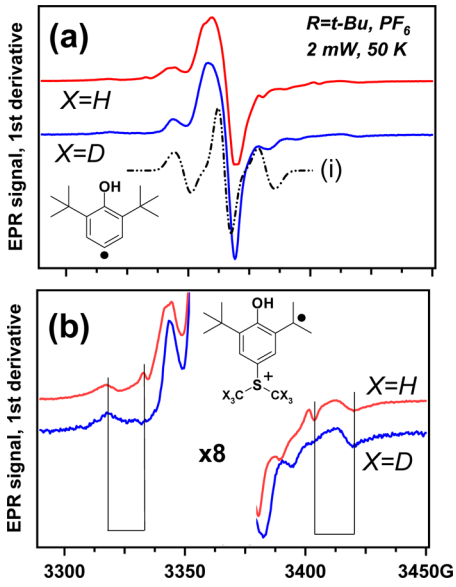

Figure 3. (a) Comparison of normalized EPR spectra from irradiated **1b**-h_6 and **1b**-d_6 hexafluorophosphate (50 K). The dashed line is the simulated EPR spectrum of the $^{\bullet}$ArOH radical shown in the inset. (b) Magnified spectral wings from panel a. The vertical lines indicate the outer resonance lines from the $Me_2Y^{\bullet}$ radical shown in the inset. The reduced number of resonance lines is caused by hindered rotation of methyl groups in this radical.

from the S−Me group does not occur, as otherwise there would be an observable difference between these two isotopomers (Figure 16S and Table 8S, Supporting Information). The EPR spectrum can be rationalized as a sum of at least three contributions: (i) the singlet line from the $^{\bullet}OArS^{+}Me_2$ radical (Figure 17S, Supporting Information), (ii) the triplet from $^{\bullet}$ArOH (Figure 18S, Supporting Information), and (iii) the set of outer lines shown at greater magnification in Figure 3b that can only belong to an $Me_2Y^{\bullet}$ radical with C_{2v} symmetry and arrested methyl group rotation (where Y is a non-magnetic nucleus). Figure 17S (Supporting Information) illustrates the effect of arrested rotation on the spectrum, that transforms a 7-line spectrum (for freely and independently rotating methyl groups) into a 5-line spectrum. The cause for this transformation is negligible hfcc's for in-plane protons of the two methyl groups and $a_{iso}(^1H) \approx 23-26$ G for protons in the off-plane protons in these groups, with $B_{cc} \approx 2$ G. Only the outer lines can be observed in our EPR spectra, as the $M = 0$ transition is obscured by other organic radicals generated in radiolysis.

Since $Me_2S^{+\bullet}$ is excluded from consideration by the d_6-substitution experiment, this $Me_2Y^{\bullet}$ radical can only be a radical resulting from methyl loss in the *tert*-butyl group of cation **1b**. We have observed previously such C−C bond dissociation in radiolysis of other *tert*-butylated aromatic cations.[29] The same radicals are observed in irradiated bistriflimide compound (Figure 18S, Supporting Information), and in both of these ionic compounds, the radicals observed at 50 K persist after 300 K annealing (Figure 19S and 20S, Supporting Information). Remarkably, no H atom adducts were observed. This would be expected if the released H atoms abstract hydroxyl protons instead of adding to the (heavily substituted) aromatic ring. In some systems, these H adducts can also be generated by protonation of the electron adducts of cations (see above).[29,30]

Apparently, this does not occur in radiolysis of cation **1b**, suggesting the facility of C−S dissociation via reaction 6a.

Turning to cation **1a**, Figure 4 exhibits the remarkable contrast of EPR spectra observed for irradiation compounds of

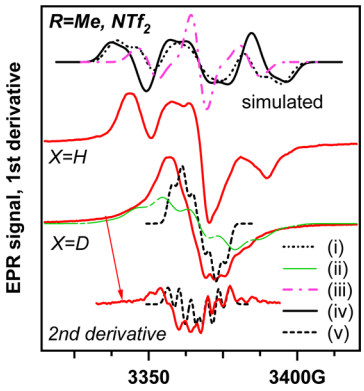

Figure 4. Simulated and observed first-derivative EPR spectra for radicals in irradiated **1a**-h_6 and **1a**-d_6 bistriflimide (50 K). Trace i is an H atom loss radical at carbon-5 (Scheme 3), trace ii is assigned to an H atom loss radical at the hydroxyl group, trace iii is $^{\bullet}$ArOH, and traces iv and v are attributed to H atom loss radicals at carbon-6, for h_6 and d_6 isotopomers, respectively. At the bottom is the second derivative EPR spectrum for the d_6 isotopomer, with the derivative of trace v overlaid.

this cation with those in Figure 3. Indeed, for **1a** (but not **1b**), there are significant differences between the EPR spectra obtained for h_6- and d_6-isotopomers. The h_6 isotopomer yields a triplet, whereas the d_6-isotopomer yields a singlet. A closer inspection of the second-derivative EPR spectrum shown at the bottom of Figure 4 suggests the involvement of the $HOArS^{+}(Me)C^{\bullet}H_2$ radical generated via H atom loss from an S−Me group; there is also a hint of the $^{\bullet}OArS^{+}Me_2$ radical (Figure 4). The latter contribution (which is nearly identical for the two isotopomers) is the only one that persists at 300 K (Figure 21S, Supporting Information), as can be expected for this aroxy radical. The same behavior was observed for the hexafluorophosphate compound of **1a** (Figure 22S, Supporting Information) for which the $HOArS^{+}(Me)C^{\bullet}H_2$ radical survives to 200−250 K. Interestingly, in radiolysis of a chloride compound (Figure 23S(a), Supporting Information) there is not much difference between these h_6- and d_6-isotopomers, suggesting the formation of H loss radicals in the C−Me groups at carbon-3. This can be rationalized through the occurrence of H abstraction by the $Cl^{\bullet}$ atoms released via electron detachment from the chloride anion.[39,61]

Finally, in parts 1 and 2 of this series,[1,2] we demonstrated that dissociative electron attachment reactions analogous to reaction 4b and 6a can be suppressed through the use of suitable electron scavenging anions, such as saccharinate (see inset in Figure 23S(b), Supporting Information). As shown in this plot, the same reactions occur in radiolysis of the saccharinate of cation **1a**.

3.2. Mass Spectrometry and NMR Spectroscopy Analyses of Cation Stability. For analyses of stable products, hexafluorophosphate compounds were used, as our previous research indicated minimal formation of products arising from the attack anion fragments on the parent cation in such compounds.[2] Our examination proceeds in the same order as section 3.1 above. We emphasize that much higher radiation doses were used in our product analysis studies than in low-temperature EPR studies, as the latter method is one of the

dx.doi.org/10.1021/jp408252n | J. Phys. Chem. B 2013, 117, 14797−14807

most sensitive spectroscopic techniques, whereas for analytical studies sufficient conversion of the starting material is required. As the latter depends on radiation stability of ions, high radiation doses are required precisely for those systems that exhibit the highest radiation stability.

Importantly, all cations shown in Scheme 3 fragment during electrospraying and collisional excitation. Scheme 6 summarizes

Scheme 6. Bond Cleavage in Excited Cations 1−4

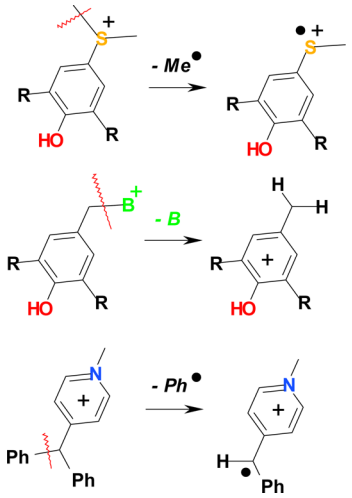

the main fragmentation pathways. For cations **1a** and **1b**, it is the elimination of methyl radical via the dissociation of the C_6−S bond

$$HOArS^+Me_2 \rightarrow\rightarrow HOArSMe^{+\bullet} + {}^\bullet CH_3 \quad (7)$$

For cations **2** and **3**, it is elimination of the $^+CH_2ArOH$ carbocation (analogous to reaction 1a)[62]

$$\mathbf{B}^+CH_2ArOH \rightarrow\rightarrow \mathbf{B} + {}^+CH_2ArOH$$

For cation **4**, it is loss of the phenyl radical

$$Ph_2CHPyMe^+ \rightarrow\rightarrow Ph_2C^\bullet HPyMe^+ + Ph^\bullet \quad (8)$$

Our DFT calculations indicate that the fragmentation always favors the lowest energy pathway. The MS_1^+ spectra of irradiated ionic compounds are summarized in Figures 24S−27S and Table 9S (Supporting Information). In the following, radiolytic yield (G) is given in species per 100 eV of the absorbed energy.

While radiolytic damage of PF_6^- anion resulting in the loss of the *cation* is a relatively minor issue for these compounds, ^{19}F and ^{31}P NMR spectroscopy (Tables 9S and 10S, Supporting Information) indicates significant *anion* loss with the formation of $PO_2F_2^-$ and PO_3F^{2-} anions that are known products of PF_6^- hydrolysis.[2] It is likely that radiolysis breaks P−F bonds in the anion, and the resulting intermediates are hydrolyzed by traces of water present in organic solvents used for analysis.

3.2.1. 1-(3,5-Ditert-butyl-4-hydroxybenzyl)pyridinium. Figure 24S (Supporting Information) shows MS_1^+ spectra for irradiated Py-x_5-CH_2ArOH PF_6. The main radiolytic product is a "quinone-like" cation Py^+CHArO ($G \sim 0.62$, see Table 9S, Supporting Information), which originates through simultaneous hydrogen loss in the −OH and $-CH_2$ groups, suggesting radical disproportionation of aroxy radicals (section 3.1.1) observed by EPR, reaction 9

$$2Py^+CH_2ArO^\bullet \rightarrow Py^+CH_2ArOH + Py^+CHArO \quad (9)$$

Such reactions are known in photochemistry and radiation chemistry of phenolic compounds.[41,63−65] Another route for decomposition involves the *tert*-butyl group of the cation, which undergoes the loss of methane ($G \sim 0.15$) or elimination of the entire group ($G \sim 0.15$). There is almost no $N-C_{1'}$ bond dissociation ($G < 0.03$, judging from the yield of the pyridine adduct); most of other radiolytic products observed are adducts of fragments of the *tert*-butyl group. The total loss of parent cation is ∼1.33 per 100 eV, which is one of the lowest decomposition yields observed. ^1H NMR spectra of the h_6-isotopomer (Figures 28S and 29S, Supporting Information) indicate the formation of a radiolytic product ($G \sim 0.63$) with a pyridinium headgroup (observed as downshifted resonance lines at 8.83, 8.37, and 7.88 ppm with dd, tt, and dd coupling patterns, which are not observed for the d_6-isotopomer, Figure 29S, Supporting Information) whose yield approximately matches the yield of Py^+CHArO that is observed in the MS_1^+ spectra. The 2.09 and 9.78 ppm lines are from acetaldehyde; the 6.88 and 7.07 ppm resonance lines that correlate with the 4.24 and 4.36 ppm lines are likely to belong to Py^+CHArO product present in *cis*- and *trans*-conformations. These ^1H NMR spectra are suggestive of relatively low radiation damage in the parent cation.

3.2.2. 1-Methyl-4-diphenylmethylpyridinium. Figure 25S (Supporting Information) shows MS_1^+ spectra for irradiated **4** TfO and **4** PF_6. The main radiolytic products correspond to methyl loss (Ph_2CHPyH^+) and $Ph^\bullet$ elimination (totaling $G \sim 0.12$). There is also a product with m/z +260.3 ($G \sim 0.33$) and adducts of the $-CH_2PyH$ and $-CH_2PyMe$, as well as adducts of phenyl and methyl radicals, all with low yield. In the triflate compound, there is significant yield of −F and $-CF_3$ modification, which results in a greater depletion of the parent cation (2.03 vs 1.2 per 100 eV). Unlike cation **3**, cation **4** does not have a preferred degradation pathway.

This is also suggested by ^1H NMR and $^1H-^1H$ COSY spectra shown in Figures 30S−32S (Supporting Information). It is seen that both irradiated compounds, **4** TfO and **4** PF_6, yield similar ^1H NMR spectra, suggesting common chemistry. Closer scrutiny of these ^1H NMR spectra (Figure 31S, Supporting Information) reveals the presence of three products with different pyridine/pyridinium moieties. Using $^1H-^1H$ COSY spectroscopy, these resonance lines can be classified into three groups of coupled protons (groups A−C shown in Figure 32S, Supporting Information) with G of 0.3, 0.6, and 0.76, respectively. In addition to these three groups, there is another set of coupled protons (group D in Figure 32S, Supporting Information) with chemical shifts corresponding to olefinic hydrogens; this set may or may not be related to groups A−C (as the continuity of proton coupling is interrupted by nitrogen atom). Group A is matched by a $-PyH^+$ headgroup, group B corresponds to a modified $-PyMe^+$ headgroup, and group C may arise through a neutral pyridine or $-C_5H_4NMe$ group (with downshifted N−Me resonance at 4.04 ppm). Such a product can occur through radiolytically induced deprotonation of the cation, reaction 10 (Scheme 7)

$$Ph_2CHPyMe^+\ \mathbf{A}^- \rightarrow\rightarrow Ph_2CC_5H_4Me + H^{\delta+}\mathbf{A}^{\delta-} \quad (10)$$

The corresponding neutral product ($Ph_2CC_5H_4Me$) may escape MS_1^+ detection, as it becomes protonated back to the parent cation during electrospraying, becoming indistinguishable from the parent cation. Assuming the latter, the total

dx.doi.org/10.1021/jp408252n | J. Phys. Chem. B 2013, 117, 14797−14807

Scheme 7. Deprotonation in Excited 1-Methyl-4-diphenylmethylpyridinium

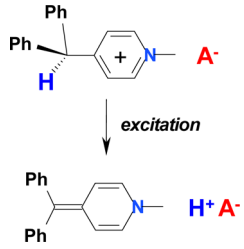

depletion of the parent cation is ~2 per 100 eV. Note that reaction 9 is reversed by contact with acids, so the actual depletion of cation **4** under practically relevant IL diluent conditions is significantly lower than this estimate and closer to our MS_1^+ estimate.

EPR observations in section 3.1.2 suggested $Ph_2C^{\bullet}PyMe^+$ radical as the main product of radiolytic oxidation. Trityl radicals decay mainly through the formation of a C−C bond between the carbon center and *para*-carbon in aromatic groups, whereas diarylpyridinemethyl radicals are known to react by addition of this carbon center to nitrogen.[43] It appears (Table 9S, Supporting Information) that the yield of such dimers is relatively low ($G \sim 0.1$) and $Ph_2C^{\bullet}PyMe^+$ radicals decay via cross-recombination involving small fragments. The predominant cation product (m/z 260 mass peak) is formally the product of methane addition to the parent cation that may originate through disproportionation of the corresponding methyl radical adducts.

3.2.3. 3,5-Dialkyl-4-hydroxyphenyldimethylsulfonium. Figures 26S and 27S (Supporting Information) exhibit MS_1^+ spectra for hexafluorophosphates of h_6- and d_6-isotopomers of **1a** and **1b**. It is seen from Figure 26S (Supporting Information) that radiation stability of cation **1a** is low, with many S−C_1 and S−Me fragments appearing in the mass spectrum along with the products of addition of these fragments to the aromatic ring of the parent cation. The identity of most of these products can be determined by comparison of two isotopomers (Table 9S, Supporting Information).

The products with the largest yield are $(HOAr)_2S^+Me$ cations and adducts of methyl, ArOH, and MeSArOH radicals. The yield of these products is so high and the parent cation is so unstable that we were unable to determine G values for cation decomposition from these mass spectra (the values in Table 9S (Supporting Information) have been calculated assuming no fragmentation in the parent cation during MS_1^+ analysis). Certainly, **1a** is one of the least stable cations we have examined so far. According to ^1H NMR, the main product of radiolytic decomposition ($G \sim 2.77$) has a chemical shift of 6.89 ppm for H_3 protons (Figure 33S, Supporting Information), suggesting the formation of $O^-ArS^+Me_2$ zwitterion via reaction 3, which may explain the untrustworthiness of our MS_1 data, as a fraction of parent cations deprotonates during the ESI/MS_1^+, increasing the apparent yield of radiolytic products relative to this parent ion.

In comparison, cation **1b** appears to be much more stable (Figure 27S, Supporting Information). Consistent with EPR observation in section 3.1.3, there is significant fragmentation in the *tert*-butyl group, with the loss of the methyl group and isobutylene, and there are adducts of the methyl and *tert*-butyl groups. The yield of adducts involving S−C_1 bond fragments is low ($G \sim 0.15$), and our MS_1^+ estimate for the depletion of **1b** is ~0.55 per 100 eV, which would be the lowest yield of radiolytic decomposition that we observed so far. However, ^1H and ^{13}C NMR spectra (Figures 34S and 35S, Supporting Information) indicate zwitterion formation with $G \sim 1.2$, so the total yield of radiolytic decomposition is, actually, close to 2 per 100 eV, which is comparable to that of other organic cations. It is remarkable that changing the substitution near the hydroxyl group from methyl to *tert*-butyl results in such a dramatic effect in radiation stability of the cation.

4. CONCLUDING REMARKS

In this study, we examine the strategy of improving the radiation stability of organic cations through introduction of strategically placed deprotonation sites, with the expectation that electronically excited cations would deprotonate from these sites, before or after the ejection of the electron. We designed cations **1**−**4** (Scheme 3) in such a way that the latter reaction yields persistent radicals (aroxyl and trityl). We observed these postulated radicals in matrix isolation EPR spectra of irradiated compounds, and also found the expected products of radical disproportionation. Below, we assess the successes and failures of this approach.

For cation **1a** (Scheme 3), both EPR and product analysis indicate significant fragmentation, making this cation one of the least stable cations that we studied. On the other hand, cation **1b** is quite stable, with most of the cations deprotonating from the hydroxyl group and becoming zwitterions. As the latter species can be protonated back by contact with acids, the irreversible loss of the cation occurs mainly through fragmentation in *tert*-butyl side arms, which is relatively low (~0.6 per 100 eV). The yield of S−C_1 fragmentation is negligible, whereas it is known to be very high in photoexcitation of arylsulfonium cations (section 1) and remains unacceptably high even in cation **1a**.

For cation **3**, no significant $N_{1'}$−C_1 bond fragmentation was observed in electronically excited and reduced states, and our results are suggestive of efficient deprotonation from the hydroxyl group. As a result, this cation exhibited one of the lowest decomposition yields observed (~1.3 per 100 eV), half of which is accounted for by a "quinone-like" product of disproportionation of the aroxyl radicals. Low yield of the $^+CH_2ArOH$ carbocation contrasts with efficient elimination of benzyl carbocation from 1-benzylpyridinium (part 2)[2] and the ease of deprotonation in the carbocation itself. While it is possible that we "missed" adducts of this carbocation for the latter reason, NMR spectroscopy does not support the formation of free pyridine or pyridinium in the radiolyzate. It seems, therefore, that cation **3** is resilient to electronic excitation, and this propensity can be rationalized assuming that the excess electronic energy is released through H−O bond dissociation as opposed to $N_{1'}$−C_1 bond dissociation. In the gas phase, the energies of these two bonds are estimated to be 3.86 vs 1.31 eV, respectively; however, the average energy per excitation/ionization events in radiolytic spurs is 5−10 eV, so it is sufficient to break the O−H bonds in preference to the $N_{1'}$−C_1 bonds. We remind that many of these excited states are generated through recombination of excess charges generated in the ionization events rather than by direct excitation, and rapid deprotonation of "holes" from their hydroxyl groups can account for the observed suppression of the $N_{1'}$−C_1 bond fission.

dx.doi.org/10.1021/jp408252n | J. Phys. Chem. B 2013, 117, 14797−14807

While cations **1b** and **3** are remarkably stable in radiolysis (and this stability only increases by contact with acids reversing zwitterion formation for **1b** and diverting radiolytic reduction for **3**), the obvious detriment of these designs is that the aroxyl groups can be oxidized by 1−5 M nitric acid, so ILs based on such cations cannot be used for radionuclide extraction from nitric acid raffinates, which are common in nuclear separations. It is also noteworthy that, to suppress the formation of phenolates of metal cations, sufficiently low pH is required. In this sense, cation **4** is more practical. EPR spectra suggest that radiolysis of this cation yields stable trityl radicals, and NMR spectra suggest the occurrence of deprotonation in the excited state. As this reaction is reversible under acidic conditions, the radiolytic yield of irreversible decomposition is as low as 1.2 per 100 eV.

The frustrating problem with these "antioxidant" designs, from an applications standpoint, is that these cations do not produce room-temperature ILs with the typical hydrophobic anions used in IL syntheses. Commonly, the melting points of ionic compounds can be lowered through introduction of long aliphatic arms into the cations,[4,5] but such designs need to be avoided to prevent fission of C−N and C−C bonds in these arms. It is possible that using more flexible anions can remedy this situation, but even if that proves impossible, such cations can serve as antioxidant, antirad additives to IL and molecular diluents and electrolytes.

Equally important, the propensity of these "task-specific" cations to deprotonate from their electronically excited and oxidized states makes them strong candidates for EUV and electron beam lithography when these cations are paired with bases of superacids. For cation **1a**, such uses (for UV photolithography) have already been explored by Crivello and co-workers,[18−22] and our results suggest that species with motifs of cations **2**, **3**, and **4** can also be used to this end. For this application, the tendency of these cations to yield crystalline compounds with bases of superacids (including bistriflimide, which commonly yields ILs rather than crystals with organic cations) is an asset, as the resists need to be in a very pure form and have vanishingly low vapor pressure. We urge systematic exploration of these relatively overlooked ionic compounds for electronics industry applications.

■ ASSOCIATED CONTENT

Supporting Information

A PDF file containing a list of abbreviations and reactions, Scheme 1S, Tables 1S−10S, and Figures 1S−35S with captions, including radical geometries, energy diagrams, experimental and simulated EPR spectra, and NMR spectra. This material is available free of charge via the Internet at http://pubs.acs.org.

■ AUTHOR INFORMATION

Corresponding Author

*Phone: (630) 252-9516. E-mail shkrob@anl.gov.

Notes

The authors declare no competing financial interest.

■ ACKNOWLEDGMENTS

We thank S. Chemerisov, R. Lowers, D. Quigley, S. Lopykinski, and J. Muntean for technical support. The work at Argonne was supported by the US-DOE Office of Science, Division of Chemical Sciences, Geosciences and Biosciences under Contract Nos. DE-AC02-06CH11357. Programmatic support via a DOE SISGR grant "An Integrated Basic Research Program for Advanced Nuclear Energy Separations Systems Based on Ionic Liquids" is gratefully acknowledged.

■ REFERENCES

(1) Shkrob, I. A.; Marin, T. W.; Luo, H.; Dai, S. Radiation Stability of Cations in Ionic Liquids. 1. Alkyl and Benzyl Derivatives of 5-Membered Ring Heterocycles. *J. Phys. Chem. B* **2013**, DOI: 10.1021/jp4082432.

(2) Shkrob, I. A.; Marin, T. W.; Wishart, J. F. Radiation Stability of Cations in Ionic Liquids. 2. Improved Radiation Resistance through Charge Delocalization in 1-Benzylpyridinium. *J. Phys. Chem. B* **2013**, DOI: 10.1021/jp408242b.

(3) Shkrob, I. A.; Marin, T. W.; Luo, H.; Dai, S. Radiation Stability of Cations in Ionic Liquids. 3. Cyclical Guanidinium Cations. *J. Phys. Chem. C* **2013**, DOI: 10.1021/jp408253y.

(4) Welton, T. Room-Temperature Ionic Liquids. Solvents for Synthesis and Catalysis. *Chem. Rev.* **1999**, *99*, 2071−2083.

(5) Hallett, J. P.; Welton, T. Room-Temperature Ionic Liquids: Solvents for Synthesis and Catalysis. 2. *Chem. Rev.* **2011**, *111*, 3508−3576.

(6) Plechkova, N. V.; Seddon, K. R. Applications of Ionic Liquids in the Chemical Industry. *Chem. Soc. Rev.* **2008**, *37*, 123−150.

(7) Visser, A. E.; Swatloski, R. P.; Reichert, W. M.; Mayton, R.; Sheff, S.; Wierzbicki, A.; Davis, J. H.; Rogers, R. D. Task-Specific Ionic Liquids for the Extraction of Metal Ions from Aqueous Solutions. *Chem. Commun.* **2001**, 135−136.

(8) Gutowski, K. E.; Bridges, N. J.; Cocalia, V. A.; Spear, S. K.; Visser, A. E.; Holbrey, J. D.; Davis, J. H.; Rogers, R. D., Ionic Liquid Technologies for Utilization in Nuclear-Based Separations. *Ionic Liquids: Fundamentals, Progress, Challenges and Opportunities: Transformations and Processes*; American Chemical Society: Washington, DC, 2005; Vol. *902*, pp 33−48.

(9) Stepinski, D. C.; Jensen, M. P.; Dzielawa, J. A.; Dietz, M. L. Synergistic Effects in the Facilitated Transfer of Metal Ions into Room-Temperature Ionic Liquids. *Green Chem.* **2005**, *7*, 151−158.

(10) Smiglak, M.; Metlen, A.; Rogers, R. D. The Second Evolution of Ionic Liquids: From Solvents and Separations to Advanced Materials - Energetic Examples from the Ionic Liquid Cookbook. *Acc. Chem. Res.* **2007**, 1182−1192.

(11) Vasudeva Rao, P. R.; Venkatesan, K. A.; Srinivasan, T. G. Studies on Applications of Room Temperature Ionic Liquids. *Prog. Nucl. Technol.* **2008**, *50*, 449−455.

(12) Venkatesan, A. K.; Srinivasan, T. G.; Vasudeva Rao, P. R. A Review on the Electrochemical Applications of Room Temperature Ionic Liquids in Nuclear Fuel Cycle. *J. Nucl. Radiochem. Sci.* **2009**, *10*, R1−R6.

(13) Sun, X. Q.; Luo, H. M.; Dai, S. Ionic Liquids-Based Extraction: A Promising Strategy for the Advanced Nuclear Fuel Cycle. *Chem. Rev.* **2012**, *112*, 2100−2128.

(14) Billard, I.; Ouadi, A.; Gaillard, C. Is a Universal Model to Describe Liquid−Liquid Extraction of Cations by Use of Ionic Liquids in Reach? *Dalton Trans.* **2013**, *42*, 6203−6212.

(15) Wishart, J. F.; Shkrob, I. A., The Radiation Chemistry of Ionic Liquids and Its Implications for Their Use in Nuclear Fuel Processing. In *Ionic Liquids: From Knowledge to Application*; Plechkova, N. V., Rogers, R. D., Seddon, K. R., Eds.; American Chemical Society: Washington, DC, 2009; pp 119−134.

(16) Wishart, J. F. Ionic Liquids and Ionizing Radiation: Reactivity of Highly Energetic Species. *J. Phys. Chem. Lett.* **2010**, *1*, 3225−3231.

(17) Berthon, L.; Chabronnel, M.-C., Radiolysis of Solvents Used in Nuclear Fuel Reprocessing In *Ion Exchange and Solvent Extraction, A Series of Advances*; Moyer, B. A., Ed.; CRC Press: Boca Raton, FL, 2010; Vol. *19*, pp 429−513.

(18) Crivello, J. V.; Lam, J. H. W. Photoinitated Cationic Polymerization by Dialkyl-4-Hydroxyphenolsulfonium Salts. *J. Polym. Sci., Polym. Chem. Ed.* **1980**, *18*, 1021−1034.

(19) Crivello, J. V.; Lee, J. L. Photosensitized Cationic Polymerizations Using Dialkylphenacylsulfonium and Dialkyl(4-Hydroxyphenyl)Sulfonium Salt Photoinitiators. *Macromolecules* **1981**, *14*, 3780−3813.
(20) Crivello, J. V. Cationic Polymerization - Iodonium and Sulfonium Salt Photoinitiators. *Adv. Polym. Sci.* **1984**, *62*, 2−48.
(21) Crivello, J. V. The Discovery and Development of Onium Salt Cationic Photoinitiators. *J. Polym. Sci., Part A: Polym. Chem.* **1999**, *37*, 4241−4254.
(22) Crivello, J. V.; Ahn, J. Synthesis and Characterization of Second-Generation *S,S*-Dialkyl-*S*-(Dimethylhydroxyphenyl)Sulfonium Salt Photoinitiators. *J. Polym. Sci., Part A: Polym. Chem.* **2003**, *41*, 2556−2569.
(23) Hamazu, F.; Akashi, S.; Koizumi, T.; Takata, T.; Endo, T. Cationic Polymerization with *p*-Substituted Benzyl *p*-Hydroxyphenyl Methyl Sulfonium Salts: Effect of Substituents and Mechanistic Aspects of Initiation Reaction. *J. Polym. Sci., Part A: Polym. Chem.* **1993**, *31*, 1023−1028.
(24) Shirai, M.; Tsunooka, M. Photoacid and Photobase Generators: Chemistry and Applications to Polymeric Materials. *Prog. Polym. Sci.* **1996**, *21*, 1−45.
(25) Tagawa, S.; Nagahara, S.; Iwamoto, T.; Wakita, M.; Kozawa, T.; Yamamoto, Y.; Werst, D.; Trifunac, A. D. Radiation and Photochemistry of Onium Salt Acid Generators in Chemically Amplified Resists. *SPIE Proc.* **2000**, *3999*, 204−213.
(26) Shirai, M.; Tsunooka, M. Photoacid and Photobase Generators: Prospects and their Use in the Development of Polymeric Photosensitive Systems. *Bull. Chem. Soc. Jpn.* **1998**, *71*, 2483−2507.
(27) Bratton, D.; Yang, D.; Dai, J.; Ober, K. Recent Progress in High Resolution Lithography. *Polym. Adv. Technol.* **2006**, *17*, 94−103.
(28) Marin, T. W.; Shkrob, I. A.; Dietz, M. L. Hydrogen-Bonding Interactions and Protic Equilibria in Room-Temperature Ionic Liquids Containing Crown Ethers. *J. Phys. Chem. B* **2011**, *115*, 3912−3918.
(29) Shkrob, I. A.; Marin, T. W.; Chemerisov, S. D.; Hatcher, J. L.; Wishart, J. F. Radiation Induced Redox Reactions and Fragmentation of Constituent Ions in Ionic Liquids. 2. Imidazolium Cations. *J. Phys. Chem. B* **2011**, *115*, 3889−3902.
(30) Shkrob, I. A.; Wishart, J. F. Free Radical Chemistry in Room-Temperature Ionic Liquids. In *Encyclopedia of Radicals in Chemistry, Biology and Materials*; Chatgilialoglu, C., Studer, A., Eds.; John Wiley & Sons, Ltd.: Chichester, U.K., 2012; pp 433−448.
(31) Dektar, J. L.; Hacker, N. P. Photochemistry of Triarylsulfonium Salts. *J. Am. Chem. Soc.* **1990**, *112*, 6004−6015.
(32) Welsh, K. M.; Dektar, J. L.; Garcia-Garibaya, M. A.; Hacker, N. P.; Turro, N. J. Photo-CIDNP and Nanosecond Laser Flash Photolysis Studies on the Photodecomposition of Triarylsulfonium Salts. *J. Org. Chem.* **1992**, *57*, 4179−4181.
(33) Shkrob, I. A.; Chemerisov, S. D.; Wishart, J. F. The Initial Stages of Radiation Damage in Ionic Liquids and Ionic Liquid-Based Extraction Systems. *J. Phys. Chem. B* **2007**, *111*, 11786−11793.
(34) Bosse, E.; Berthon, L.; Zorz, N.; Monget, J.; Berthon, C.; Bisel, I.; Legand, S.; Moisy, P. Stability of $[MeBu_3N][Tf_2N]$ under Gamma Irradiation. *Dalton Trans.* **2008**, 924−931.
(35) Berthon, L.; Nikitenko, S. I.; Bisel, I.; Berthon, C.; Faucon, M.; Saucerotte, B.; Zorz, N.; Moisy, P. Influence of Gamma Irradiation on Hydrophobic Room-Temperature Ionic Liquids [BuMeIm] PF_6 and $[BuMeIm](CF_3SO_2)_2N$. *Dalton Trans.* **2006**, 2526−2534.
(36) Le Rouzo, G.; Lamouroux, C.; Dauvois, V.; Dannoux, A.; Legand, S.; Durand, D.; Moisy, P.; G., M. Anion Effect on Radiochemical Stability of Room-Temperature Ionic Liquids under Gamma Irradiation. *Dalton Trans.* **2009**, 6175−6184.
(37) Wu, H.; Gonsalves, K. E. Novel Positive-Tone Chemically Amplified Resists with Photoacid Generator in the Polymer Chains. *Adv. Mater.* **2001**, *13*, 670−672.
(38) Huang, W.; Chen, S.; Liu, Y.; Fu, H.; Wu, G. Fluoride Ion Yield and Absorption Spectral Analysis of Irradiated Imidazolium-Based Room-Temperature Ionic Liquids. *Radiat. Phys. Chem.* **2011**, *80*, 573−577.
(39) Shkrob, I. A.; Marin, T. W.; Chemerisov, S. D.; Wishart, J. F. Radiation-Induced Redox Reactions and Fragmentation of Constituent Ions in Ionic Liquids. I. Anions. *J. Phys. Chem. B* **2011**, *115*, 3872−3888.
(40) Shkrob, I. A.; Marin, T. W.; Wishart, J. F. Ionic Liquids Based on Polynitrile Anions: Hydrophobicity, Low Proton Affinity, and High Radiolytic Resistance Combined. *J. Phys. Chem. B* **2013**, *117*, 7084−7094.
(41) Altwicker, E. R. The Chemistry of Stable Phenoxy Radicals. *Chem. Rev.* **1967**, *67*, 475−531.
(42) Gugumus, F. *Oxidation Inhibition in Organic Materials*; CRC Press: Boca Raton, FL, 1990; Vol. *1*.
(43) Tidwell, T. T. Triarylmethyl and Related Radicals. In *Stable Radicals: Fundamentals and Applied Aspects of Odd-Electron Compounds*; Hicks, R., Ed.; John Wiley & Sons: Chichester, U.K., 2011; pp 1−31.
(44) Davis, J. H. Task-Specific Ionic Liquids. *Chem. Lett.* **2004**, *33*, 1072−1077.
(45) Giernoth, R. Task-Specific Ionic Liquids. *Angew. Chem., Int. Ed.* **2010**, *49*, 2834−2839.
(46) Lee, S. Functionalized Imidazolium Salts for Task-Specific Ionic Liquids and Their Applications. *Chem. Commun.* **2006**, 1049−1063.
(47) Mohapatra, P. K.; Sengupta, A.; Iqbal, M.; Huskens, J.; Verboom, W. Highly Efficient Diglycolamide-Based Task-Specific Ionic Liquids: Synthesis, Unusual Extraction Behaviour, Irradiation, and Fluorescence Studies. *Chem.—Eur. J.* **2013**, *19*, 3230−3238.
(48) Nockemann, P.; Thijs, B.; Pittois, S.; Thoen, J.; Glorieux, C.; Van Hecke, K.; Van Meervelt, L.; Kirchner, B.; Binnemans, K. Task-Specific Ionic Liquid for Solubilizing Metal Oxides. *J. Phys. Chem. B* **2006**, *110*, 20978−20992.
(49) Nockemann, P.; Thijs, B.; Parac-Vogt, T. N.; Hecke, K. V.; Meervelt, L. V.; Tinant, B.; Hartenbach, I.; Schleid, T.; Ngan, V. T.; Nguyen, M. T.; Binnemans, K. Carboxyl-Functionalized Task-Specific Ionic Liquids for Solubilizing Metal Oxides. *Inorg. Chem.* **2008**, *47*, 9987−9999.
(50) Sawant, A. D.; Raut, D. G.; Darvatkar, N. B.; Salunkhe, M. M. Recent Developments of Task-Specific Ionic Liquids in Organic Synthesis. *Green Chem. Lett. Rev.* **2011**, *4*, 41−54.
(51) Kim, E. J.; Koa, S. Y.; Dziadulewicz, E. K. Mitsunobu Alkylation of Imidazole: A Convenient Route to Chiral Ionic Liquids. *Tetrahedron Lett.* **2005**, *46*, 631−633.
(52) Petit, S.; Azzouz, R.; Fruit, C.; Bischoff, L.; Marsais, F. An Efficient Protocol for the Preparation of Pyridinium and Imidazolium Salts Based on the Mitsunobu Reaction. *Tetrahedron Lett.* **2008**, *49*, 3663−3665.
(53) Anderson, L. C.; Seeger, N. V. The Absorption Spectra of Some Methylpyridine Derivatives. *J. Am. Chem. Soc.* **1949**, *71*, 343−345.
(54) Berson, J. A.; Evleth, E. M.; Hamlet, Z. Nitrogen Analogs of Sesquifulvalene. I. Synthesis and Properties. *J. Am. Chem. Soc.* **1965**, *87*, 2887−2900.
(55) Becke, A. D. Density-Functional Exchange-Energy Approximation with Correct Asymptotic Behavior. *Phys. Rev. A* **1988**, *38*, 3098−3100.
(56) Lee, C.; Yang, W.; Parr, R. G. Development of the Colle-Salvetti Correlation-Energy Formula into a Functional of the Electron Density. *Phys. Rev. B* **1988**, *37*, 785−789.
(57) Frisch, M. J.; Trucks, G. W.; Schlegel, H. B.; Scuseria, G. E.; Robb, M. A.; Cheeseman, V. G.; Montgomery, J. A., Jr.; Vreven, K. N.; Kudin, J. C.; Burant, J. C. *Gaussian 03*, rev. C.02; Gaussian, Inc.: Wallingford, CT, 2004.
(58) Shkrob, I. A. Deprotonation and Oligomerization in Photo-, Radiolytically, and Electrochemically Induced Redox Reactions in Hydrophobic Alkylalkylimidazolium Ionic Liquids. *J. Phys. Chem. B* **2010**, *114*, 368−375.
(59) Shkrob, I. A.; Marin, T. W.; Chemerisov, S. D.; Wishart, J. F. Radiation and Radical Chemistry of NO_3^-, HNO_3, and Dialkylphosphoric Acids in Room-Temperature Ionic Liquids. *J. Phys. Chem. B* **2011**, *115*, 10927−10942.

(60) Shkrob, I. A.; Trifunac, A. D. Pulsed Radiolysis of Alkanes. A Time-Resolved EPR Study. Part II. Phenolic Additives. *Radiat. Phys. Chem.* **1995**, *46*, 97−104.
(61) Shkrob, I. A.; Marin, T. W.; Crowell, R. A.; Wishart, J. F. Photo- and Radiation- Chemistry of Halide Anions in Ionic Liquids. *J. Phys. Chem. B* **2013**, *117*, 5742−5756.
(62) Barylyuk, K. V.; Chingin, K.; Balabin, R. M.; Zenobi, R. Fragmentation of Benzylpyridinium "Thermometer" Ions and Its Effect on the Accuracy of Internal Energy Calibration. *J. Am. Soc. Mass Spectrom.* **2010**, *21*, 172−177.
(63) Land, E. J.; Ebert, M. Pulse Radiolysis Studies of Aqueous Phenol. Water Elimination from Dihydroxycyclohexadienyl Radicals to Form Phenoxyl. *Trans. Faraday Soc.* **1967**, *1967*, 1181−1190.
(64) Stebbins, R.; Sicilio, F. The Kinetics of Disproportionation of the 2,6-Di-*tert*-Butyl-4-Methyl Phenoxy Radical. *Tetrahedron* **1970**, *26*, 291−297.
(65) Roginskii, V. A.; Krasheninnikova, G. A. ESR Spectra and Kinetics of the Disproportionation of Substituted Phenoxyl Radicals. II. Cross-Disproportionation in a System Containing Two Phenols. *Kinet. Catal.* **1987**, *28*, 305−312.